JOURNAL OF SOLID STATE CHEMISTRY 50, 111–120 (1983)

Simultaneous Measurements of Oxygen Pressure, Composition, and Electrical Conductivity in Praseodymium Oxides: II. $Pr_{10}O_{18}$ and PrO_{2-x} Phases

HIDEAKI INABA AND KEIJI NAITO

Department of Nuclear Engineering, Faculty of Engineering, Nagoya University, Furo-cho, Chikusa-ku, Nagoya, Japan

Received March 24, 1983; in revised form June 23, 1983

Simultaneous measurements of oxygen pressure, composition, and electrical conductivity have been conducted in $Pr_{10}O_{18\pm x}$ (epsilon) and PrO_{2-x} (alpha) phases, between $Pr_9O_{16\pm x}$ (zeta) and $Pr_{10}O_{18\pm x}$ phases, and between $Pr_7O_{12\pm x}$ (iota) and PrO_{2-x} phases. In $Pr_{10}O_{18\pm x}$ phase, the predominant defects are assigned to be neutral oxygen interstitials and neutral or doubly charged oxygen vacancies, and electrical conduction is thought to be governed mainly by the concentration of 7-coordinated praseodymium ions, which are the easiest sites for hopping electrons between Pr^{3+} and Pr^{4+} ions. In PrO_{2-x} phase, the electrical conductivity increases with oxygen pressure and the O/Pr ratio and the predominant defects are assigned to be neutral oxygen interstitials, indicating that oxygen vacancies are ordered in a short range and this phase is expressed by $PrO_{1.78+x}$ rather than PrO_{2-x} in the region measured. The electrical conductivity-composition measurement, as well as the oxygen pressure-composition measurement, shows a reproducible hysteresis loop between $Pr_9O_{16\pm x}$ and $Pr_{10}O_{18\pm x}$ and it is discussed in terms of a domain model.

1. Introduction

The intermediate praseodymium oxides form a fluorite-related homologous series, Pr_nO_{2n-2}, with a narrow range of nonstoichiometry and ordered structures at low temperatures (*1–3*). An epsilon ($n = 10$) phase belongs to this homologous series with ordered oxygen vacancies along $\langle 21\bar{1}\rangle_F$ forming a superlattice, but its *b* and *c* axes are different from odd numbered members such as the iota ($n = 7$) and zeta ($n = 9$) phases (*1*). At higher temperatures and higher oxygen pressures, a widely nonstoichiometric disordered phase, PrO_{2-x} (alpha), with the fluorite structure (*3–5*) becomes stable. The phase diagram of praseodymium oxides system by Hyde *et al.* (*3*) has been shown in the preceding paper (*6*).

In the preceding study (*6*), the defect structures and the mechanism of electron conduction in $Pr_7O_{12\pm x}$ and $Pr_9O_{16\pm x}$ phases and the hysteresis between Pr_7O_{12} and Pr_9O_{16} phases have been discussed on the basis of the results of simultaneous measurements of oxygen pressure, composition, and electrical conductivity. From the composition-pressure relation and the pressure dependence of the diffusion constant (*7*), the predominant defects in $Pr_7O_{12\pm x}$ and $Pr_9O_{16\pm x}$ phases have been thought to be neutral oxygen interstitials and doubly charged oxygen vacancies. From the electrical conductivity-composition relation, it has been found that the electrical conduc-

0022-4596/83 $3.00

tivity shows a maximum at the hyperstoichiometric Pr_7O_{12+x} and a minimum at the hypostoichiometric Pr_9O_{16-x}. This behavior has been discussed on the basis of the hopping mechanism (*8–10*) between the ordered sites Pr^{3+} and Pr^{4+} in the $Pr_7O_{12\pm x}$ and $Pr_9O_{16\pm x}$ phases (*6*).

The composition-pressure measurements of phase transformations between the intermediate phases have shown that reproducible hysteresis loops are found when the phase reaction cycle is completed between two phases (*3–6, 13–18*). A hysteresis in the electrical conductivity-pressure measurement between the iota and zeta phases as well as in the composition-pressure measurement was observed in the preceding study and it has been discussed in terms of a domain model in the two-phase region (*6*).

In this paper, simultaneous measurements of oxygen pressure, composition, and electrical conductivity have been made in the $Pr_{10}O_{18\pm x}$ and PrO_{2-x} phases, between the $Pr_9O_{16\pm x}$ and $Pr_{10}O_{18\pm x}$ phases, and between the $Pr_7O_{12\pm x}$ and PrO_{2-x} phases, and the defect structure, electrical conduction, and the hysteresis loop in these phases have been discussed from the results of the three simultaneous measurements.

2. Experimental

Oxygen vapor pressure and the O/Pr ratio were determined by the pressure measurement with a mercury manometer and the electrical conductivity was measured by the usual four probe method, simultaneously. To obtain the good sensitivity in the O/Pr ratio measurement, the sample amount and the dead volume of a sample tube were taken as much as possible and as small as possible, respectively. The details of the apparatus and the sample have been described in the preceding paper (*6*).

3. Results

Simultaneous measurements of oxygen pressure, composition, and electrical conductivity were made for the epsilon phase ($Pr_{10}O_{18\pm x}$) along oxidation and reduction paths in an isothermal condition at 778 K, since this phase is stable only below about 800 K as seen from the phase diagram. The

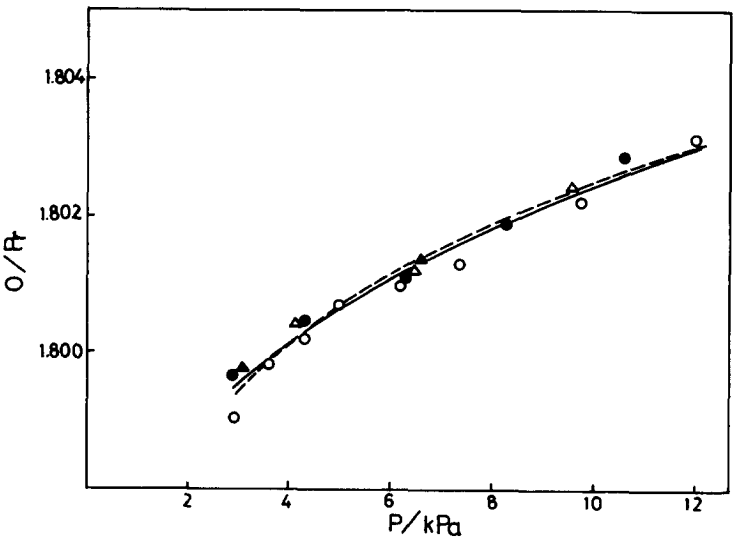

FIG. 1. Composition-pressure plot in the epsilon phase ($Pr_{10}O_{18\pm x}$) at 778 K; ○, △ oxidation; ●, ▲ reduction. A solid line and a broken line represent Eqs. (1) and (2), respectively.

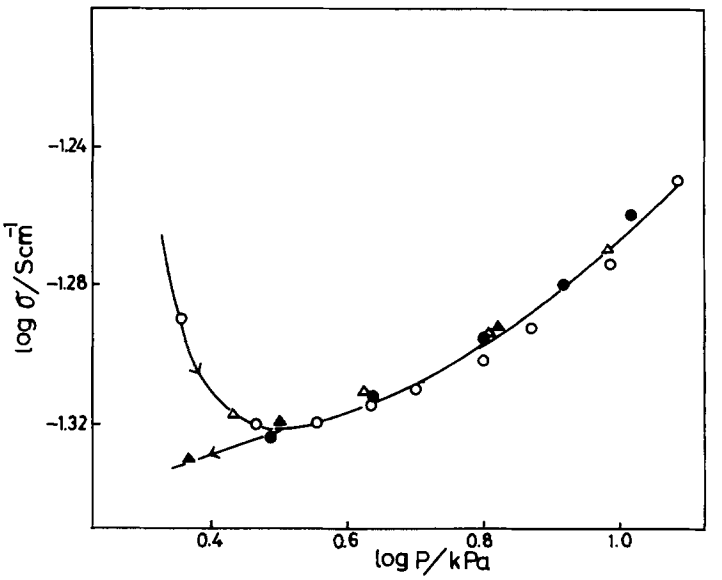

FIG. 2. Electrical conductivity-pressure plot in the epsilon phase at 778 K; ○, △ oxidation; ●, ▲ reduction.

composition-pressure and electrical conductivity-pressure relations are shown in Figs. 1 and 2, respectively. The O/Pr ratio was determined as a deviation from 1.714, which is taken as a reference at 808 K and 13.3 Pa in the same way as described in the previous paper (*16*). The composition-pressure relation is similar to the cases for $Pr_7O_{12\pm x}$ and $Pr_9O_{16\pm x}$, but the electrical conductivity-pressure relation is different from the cases for $Pr_7O_{12\pm x}$ and $Pr_9O_{16\pm x}$; log σ–log P plot shown in Fig. 2 does not show a linear relationship and the slope is somewhat larger compared with the cases of $Pr_7O_{12\pm x}$ and $Pr_9O_{16\pm x}$. At low pressures, a hysteresis between oxidation and reduction paths is seen in Fig. 2 which is due to the appearance of two-phase mixture of the zeta ($Pr_9O_{16\pm x}$) and epsilon ($Pr_{10}O_{18-x}$) phases.

A full isothermal hysteresis loop in the O/Pr ratio-pressure curve at 778 K was observed between the zeta and epsilon phases as shown in Fig. 3 where oxidation was started at the iota phase, but reduction ended at the zeta phase, because a reduction rate in the process from the zeta to the iota was very low at this temperature. This hysteresis loop at 778 K is in good agreement with that obtained by the thermogravimetric study by Sugihara *et al.* (*17*). The electrical conductivity-composition curve along the hysteresis loop between the zeta and epsilon phases at 778 K obtained by the simultaneous measurement is also shown in Fig. 4. It shows a behavior similar to the case between the iota and zeta phases; the conductivity shows a maximum at the $Pr_9O_{16\pm x}$ phase, decreases as the O/Pr increases in the two-phase region with a hysteresis loop, and increases again in the epsilon phase.

The composition-pressure (O/Pr-P), electrical conductivity-pressure (σ-P), and electrical conductivity-composition (σ-O/Pr) curves obtained by the simultaneous measurements at 903, 913, and 923 K for the alpha phase (PrO_{2-x}) are shown in Figs. 5, 6, and 7, respectively. The O/Pr-P plots (Fig. 5) show parabolic curves at three dif-

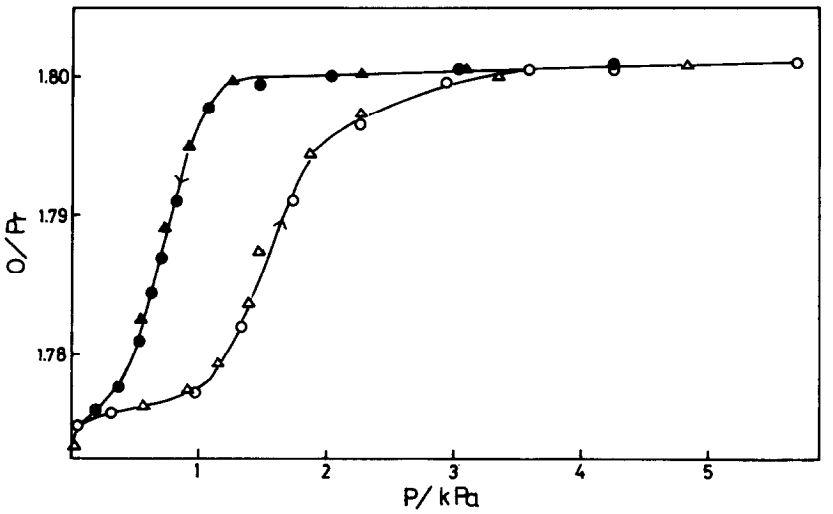

FIG. 3. Isothermal hysteresis loop between the zeta and epsilon phases at 778 K; ○, △ oxidation; ●, ▲ reduction.

ferent temperatures. The log σ-log P plots (Fig. 6) show straight lines with slopes 0.042, 0.040, and 0.041, at 903, 913, and 923 K, respectively. The log σ-O/Pr plots (Fig. 7) show that the electrical conductivity increases with the O/Pr ratio.

The O/Pr-P plot between the iota and alpha phases at 923 K is shown in Fig. 8, where a reproducible hysteresis loop is seen in the two-phase region. The hysteresis loop is wide near the iota phase and becomes narrower with the increasing O/Pr

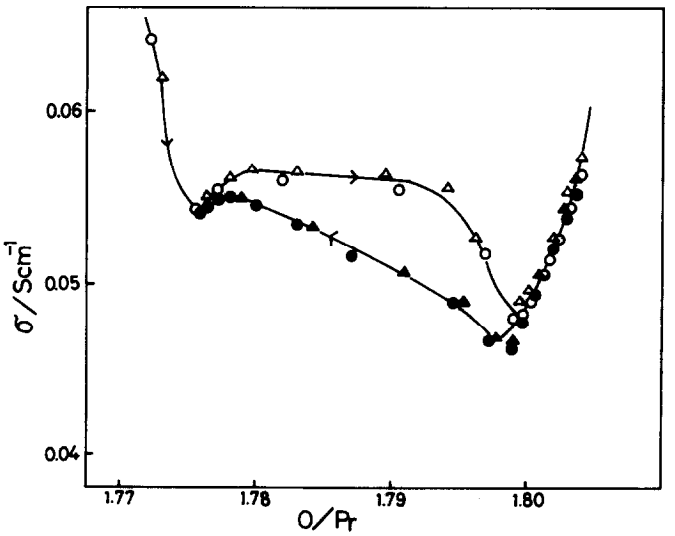

FIG. 4. Electrical conductivity of praseodymium oxides along the hysteresis loop between the zeta and epsilon phases at 778 K; ○, △ oxidation; ●, ▲ reduction.

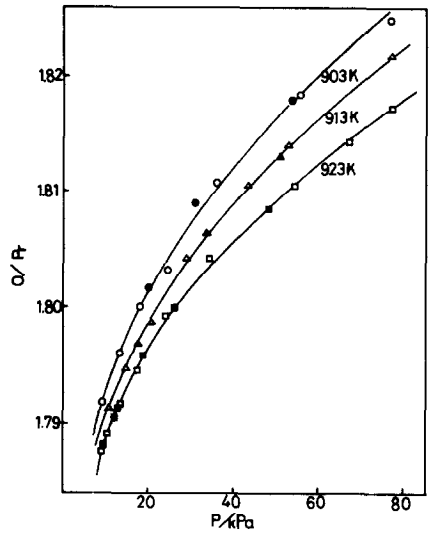

FIG. 5. Composition-pressure plot in the alpha phase at 903, 913, and 923 K; ○, △, □ oxidation; ●, ▲, ■ reduction. Solid lines represent Eq. (3).

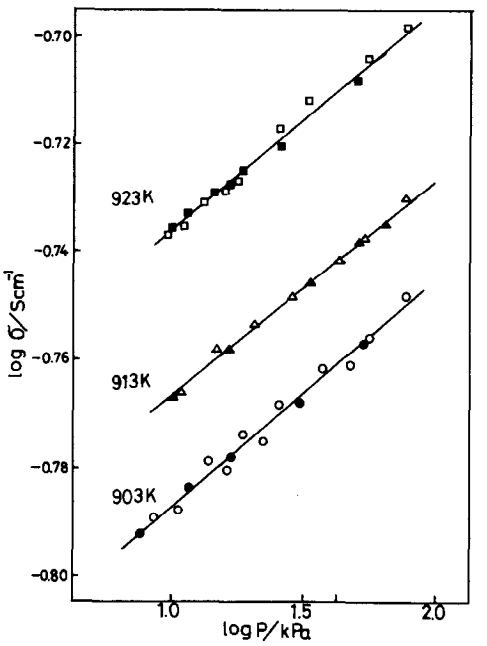

FIG. 6. Electrical conductivity-pressure plot in the alpha phase at 903, 913, and 923 K; ○, △, □ oxidation; ●, ▲, ■ reduction.

ratio, which is consistent with the one observed by the thermogravimetric study at 986 K (*5*). The conductivity-O/Pr plot between the iota and alpha phases is shown in Fig. 9; the conductivity shows a maximum in the hyperstoichiometric iota phase, and decreases slightly in the two-phase region as the O/Pr ratio increases, then increases again in the alpha phase. No hysteresis loop is observed in the two-phase region in this case.

4. Discussion

4.1 Defect Structure of the Epsilon ($Pr_{10}O_{18\pm x}$) and Alpha (PrO_{2-x}) Phases

(*a*) *Defect Structure of the Epsilon Phase*

The epsilon phase belongs to the even numbered members of homologous series Pr_nO_{2n-2}, which possess the common *a* and *c* axes, but the different *b* axis (*1*). The even and odd numbered members have the common *a* axis $\langle 21\bar{1}\rangle_F$, but are different in the *b* and *c* axes. The unit cell of $Pr_{10}O_{18}$ ($Pr_{40}O_{72}$) is made up of four pairs of oxygen vacancies per the unit cell ($Pr_{40}O_{72}$). A model for the $Pr_{10}O_{18}$ structure is shown in Fig. 10, based on the model by Tuenge and Eyring (*2*), where one-fourth of the unit cell is shown. In the nonstoichiometric epsilon

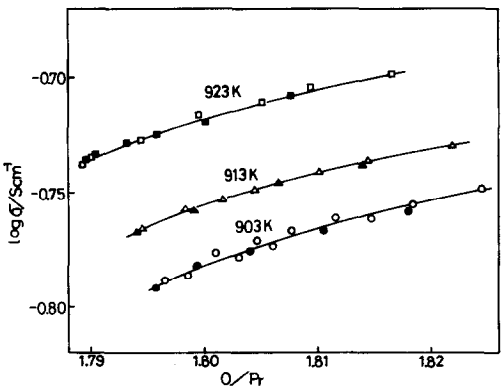

FIG. 7. Compositional dependence of the electrical conductivity in the alpha phase at 903, 913, and 923 K; ○, △, □ oxidation; ●, ▲, ■ reduction.

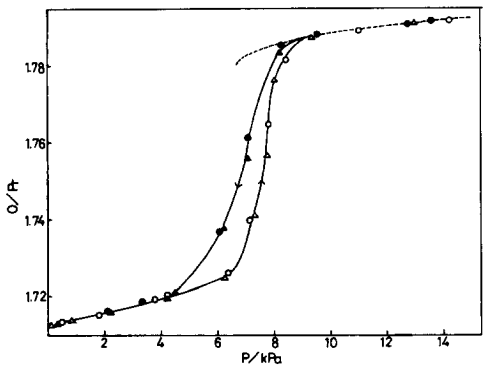

FIG. 8. Hysteresis loop between the iota and alpha phases at 923 K. A broken line represents the equilibrium or the hypothetical equilibrium curve due to Eq. (3); ○, △ oxidation; ●, ▲ reduction.

phase, the nonstoichiometric parameter δ of $PrO_{1.800+\delta}$ can be expressed by the defect model of neutral interstitials and neutral vacancies as Eq. (1), and by that of neutral interstitials and doubly charged vacancies as Eq. (2):

$$\delta = [O_i] - [V_O] = K_1 P_{O_2}^{1/2} - K_2 P_{O_2}^{-1/2}, \quad (1)$$

$$\delta = [O_i] - [V''_O] = K_1 P_{O_2}^{1/2} - K_2 P_{O_2}^{-1/6}, \quad (2)$$

where $[O_i]$, $[V_O]$, and $[V''_O]$ are the concentrations of neutral oxygen interstitials, neutral oxygen vacancies, and doubly charged oxygen vacancies, respectively, and K_1 and K_2 are constants independent of oxygen pressure. The fittings of Eqs. (1) and (2) to the composition-pressure curve are shown in broken and solid lines, respectively, in Fig. 1, where both fittings are good. It is concluded from these results that one of the point defects is assigned to be the neutral oxygen interstitial, but the charge of the oxygen vacancy cannot be determined unambiguously.

(*b*) *Defect Structure of the Alpha Phase*

The composition-pressure plots in the alpha phase (PrO_{2-x}) shown in Fig. 5 fit very well to the following parabolic equation as shown in solid lines:

$$2 - x = 1.780 + K(P - P_O)^{1/2}. \quad (3)$$

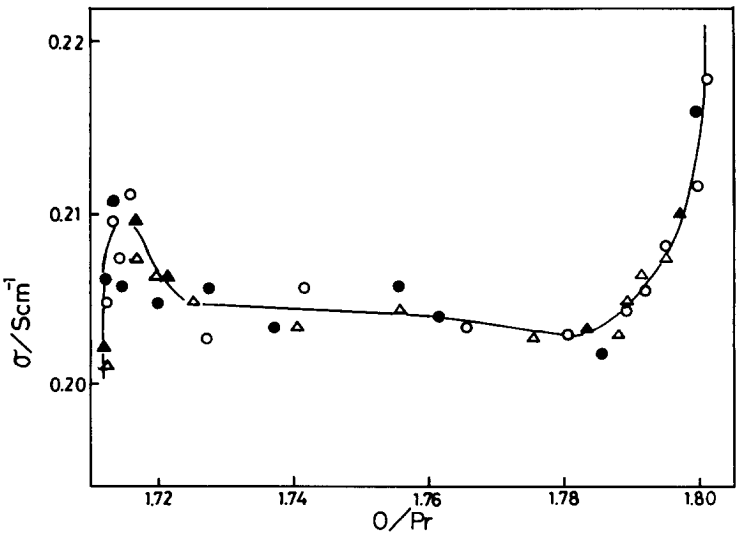

FIG. 9. Electrical conductivity of praseodymium oxides along the hysteresis loop between the iota and alpha phases at 923 K. ○, △ oxidation; ●, ▲ reduction.

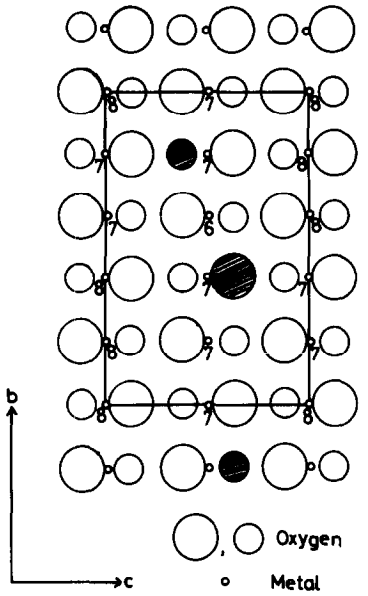

FIG. 10. A model for the structure of the epsilon phase ($Pr_{10}O_{18}$). One-fourth of the unit cell ($Pr_{40}O_{72}$) in a projection along $[2\bar{1}\bar{1}]_F = [100]_\varepsilon$ is shown. Small circles represent rows of metal atoms, and larger circles are rows of oxygen atoms, where the same size circle represents the same level. The shaded circles represent oxygen vacancies. Numbers marked at metal positions represent the coordination numbers of cations.

This relationship indicates that P_O is a hypothetical equilibrium pressure at a hypothetical stoichiometric composition O/Pr = 1.780 and it is found to be 4.7, 5.6, and 6.7 kPa at 903, 913, and 923 K, respectively; K is a constant independent of pressure found to be 5.382×10^{-3}, 4.927×10^{-3}, and 4.438×10^{-3} $Pa^{-1/2}$ at 903, 913, and 923 K, respectively. Equation (3) at 923 K is also shown in a broken line in Fig. 8 including the hypothetical equilibrium curve below 9 kPa. It is noted that the hypothetical equilibrium pressure at the hypothetical stoichiometric composition corresponds to the lowest pressure of the appearance of the alpha phase in the oxidation branch along the hysteresis loop as seen in Fig. 8. The good fitting to Eq. (3) indicates that the predominant defects of the alpha phase are neutral oxygen interstitials, since the O/Pr ratio increases with a square root of oxygen pressure. The small slopes in log σ-log P plots in the alpha phase shown in Fig. 6 would support this conclusion. Jenkins *et al.* (*19*) have suggested the presence of a short-range ordering in the alpha phase. The presence of the hypothetical stoichiometric composition $PrO_{1.780}$ would indicate that oxygen vacancies are not distributed randomly but are highly ordered in a short range probably with a structure similar to the $Pr_9O_{16\pm x}$ phase judging from its composition. The alpha phase in this region, therefore, could be expressed as $PrO_{1.780+x}$ rather than PrO_{2-x}.

4.2 Electrical Conduction in the Epsilon and Alpha Phases

(a) Comparison of the Electrical Conductivity among the Iota, Zeta, and Epsilon Phases

Honig *et al.* (*10*) measured the Seebeck coefficient and the electrical conductivity of praseodymium oxides using a single crystal sample over a wide range of the O/Pr ratio and found that the Seebeck coefficient changed its sign from negative to positive around $PrO_{1.75}$ with the increase of the O/Pr ratio and that the electrical conductivity showed a maximum around $PrO_{1.75}$. They discussed the electrical conductivity of praseodymium oxides on the basis of hopping mechanism and the assumption that Pr^{3+} and Pr^{4+} ions are randomly distributed in the praseodymium oxides (*10–12*), but our preceding study (*6*) has revealed that their model is not sufficient to describe the electrical conduction of praseodymium oxides because of the assumption that the mobility of charge carriers is independent on sites. It is then reasonable to assume in the same way as the preceding paper (*6*) that the mobilities of charge carriers are different due to the three kinds of praseodymium sites with different coordination numbers resulting from the ordered

TABLE I

RELATIONSHIP BETWEEN THE ELECTRICAL CONDUCTIVITY (σ) AND THE NUMBER OF 7-COORDINATED PRASEODYMIUM IONS PER UNIT VOLUME (Pr(7)) IN Pr_7O_{12}, Pr_9O_{16}, AND $Pr_{10}O_{18}$.

	σ (S cm^{-1})		Ratio of σ	Pr(7)[b] (nm)$^{-3}$	Ratio of Pr(7)
Pr_7O_{12}	0.141[a]	(838 K)	1.0	20.44	1.0
Pr_9O_{16}	0.115[a]	(838 K)	0.816	17.82	0.872
	0.055	(778 K)			
$Pr_{10}O_{18}$	0.048	(778 K)	0.712	14.65	0.717

[a] From Ref. (6).
[b] Calculated from the data in Ref. (1).

structures of praseodymium oxides. The coordination numbers of the ordered metal positions in the epsilon phase can be obtained from a model based on the results by Tuenge and Eyring (2), and they are marked at the metal positions in Fig. 10. Praseodymium ions of $Pr_{10}O_{18}$ in one-fourth of the unit cell are composed of

$$\text{Pr(6)} \times 1 + \text{Pr(7)} \times 6 + \text{Pr(8)} \times 3, \quad (4)$$

where Pr(n) means a praseodymium ion surrounded by n O^{2-} ions. Pr(6) is thought to correspond Pr^{3+}, Pr(8) is Pr^{4+}, Pr(7) is either Pr^{3+} or Pr^{4+} and would be regarded to be $Pr^{3.5+}$ as an average. Then for another expression of $Pr_{10}O_{18}$, we obtain

$$(Pr^{3+} \cdot Pr_6^{3.5+} \cdot Pr_3^{4+})\ O_{18}^{2-}. \quad (5)$$

Pr(7) or $Pr^{3.5+}$ site among Pr(6), Pr(7), and Pr(8) is considered to be the easiest one to jump to or from, because this site is either Pr^{3+} or Pr^{4+} and the average valence is 3.5+. Then, as a first approximation, we assume that the electrical conductivity of intermediate praseodymium oxides is proportional to the concentration of Pr(7) in a unit volume. Experimental data of the electrical conductivity and the unit cell volume for Pr_7O_{12}, Pr_9O_{16}, and $Pr_{10}O_{18}$ are listed in Table I, and the ratios of the electrical conductivities are compared with those of the concentrations of 7-coordinated praseodymium ions per a unit volume. It is seen from the table that the both ratios are in good agreement. The electrical conductivity thus can be correlated with the concentration of 7-coordinated praseodymium ions as a first approximation.

(b) *Electrical Conduction in the Nonstoichiometric Epsilon Phase*

The electrical conductivity is also thought to be dependent on the point defects in the epsilon phase, because the log σ-log P and σ-O/Pr plots show considerable increases of the electrical conductivity with oxygen pressure and the O/Pr ratio as seen in Figs. 2 and 4, respectively. The predominant point defects in the epsilon phase would be neutral oxygen interstitials according to Eqs. (1) and (2) and Fig. 1. The presence of neutral oxygen interstitials would cause an increase in the probability of hopping between Pr^{3+} and Pr^{4+} ions, but the mechanism is not clear at present.

The slope of log σ-log P plot is 0.005 in the iota phase, 0.031 in the zeta phase, and the relation becomes nonlinear with a larger slope in the epsilon phase. Although the quantitative interpretation of this fact is difficult, the increase of the electrical conductivity due to the addition of neutral oxygen atoms would be more effective for samples with the lower electrical conductivity.

(c) *Electrical Conduction in the Alpha Phase*

The log σ-log P plots shown in Fig. 6 show positive slopes and log σ in Fig. 7 increases with the O/Pr ratio in the alpha phase, where electrons are major charge carriers (n-type). These behaviors are opposite to the usual point defect model and the model proposed by Honig *et al.* (10), indicating that oxygen vacancies are not random even in the alpha phase. In the alpha phase, no long-range ordering structure

has been observed, but a short-range ordering of vacancies is suggested by Jenkins *et al.* (*19*) from the measurement of partial molar entropy of the alpha phase. Tuller and Nowick (*20*) measured the electrical conductivity of a disordered CeO_{2-x} phases as a function of the O/Ce ratio and it was found that the electrical conductivity showed a broad flat maximum around $x = 0.10$. They suggested that a high degree of a short-range order was present in the reduced fluorite phase at higher values of x, and that these locally ordered configurations served to immobilize some of the carriers. Since the alpha phase is a high temperature phase of iota ($n = 7$), zeta ($n = 9$), epsilon ($n = 10$), delta ($n = 11$), and beta ($n = 12$) in the homologous series Pr_nO_{2n-2}, the short-range ordered structure in the alpha phase would be composed of a basic unit common to the structures of the homologous series. The facts that the predominant point defects are neutral oxygen interstitials and that a log σ-log P plot showing a slight positive slope is commonly observed in the alpha phase and the low temperature phases (iota, zeta, and epsilon) would support this statement. From the structural point of view, the common feature of the homologous series is the presence of paired oxygen vacancies along ⟨111⟩ direction in the fluorite structure and these paired oxygen vacancies would be the basic unit of a short-range ordered structure in the alpha phase. The presence of paired oxygen vacancies creates various coordination numbers of praseodymium ions Pr(6), Pr(7), and Pr(8) and the concentration of Pr(7) would mainly determine the magnitude of the electrical conductivity in the alpha phase as in the phases iota, zeta, and epsilon.

4.3 Chemical Hysteresis between the Zeta and Epsilon and between the Iota and Alpha Phases

According to the preceding study (*6*), a nearly symmetrical hysteresis loop in the electrical conductivity-composition curve as well as in the composition-pressure curve has been obtained between the iota and zeta phases. It has been proposed as a domain model that islands of layers extending to c direction common to the iota and zeta lattice intergrow coherently from the matrix phase, and the islands–matrix texture is dependent on the path of the hysteresis loop. This domain model is considered to be consistent with the models on hysteresis presented previously (*18, 21–23*).

The electrical conductivity-composition curve between the zeta and epsilon phases shows a hysteresis loop similar to the case between the iota and zeta phases as shown in Fig. 4, indicating that the gross feature of the domain distribution is the same as the case between the iota and zeta phases. However, it is noted that the hysteresis loop is not symmetrical in this case; it is the widest around O/Pr = 1.794 and becomes narrower in lower and higher O/Pr compositions. An islands–matrix transition seems to occur at about 70 vol% of the zeta phase in the oxidation path, but it is not clear in the reduction path. The zeta ($n = 9$) and epsilon ($n = 10$) phases belong to the same homologous series Pr_nO_{2n-2} with the common a axis along $\langle 2\bar{1}1\rangle_F$, but possess different b and c axes, because the zeta phase belongs to the odd-numbered series and the epsilon phase belongs to the even-numbered series (*1*). The degree of coherency between the zeta and epsilon phases may not be so strong as that between the iota and zeta phase, which may result in the unsymmetrical hysteresis loop in the electrical conductivity-composition curve.

The hysteresis loop in the electrical conductivity-composition relation between the iota and alpha phases would possibly exist, but it cannot be recognized in Fig. 9, since the magnitudes of the electrical conductivity for the iota and alpha phases are nearly the same.

References

1. P. KUNZMANN AND L. EYRING, *J. Solid State Chem.* **14,** 229 (1975).
2. R. T. TUENGE AND L. EYRING, *J. Solid State Chem.* **29,** 165 (1979).
3. B. G. HYDE, D. J. M. BEVAN, AND L. EYRING, *Philos. Trans. R. Soc. London Ser. A* **259,** 583 (1966).
4. D. A. BURNHAM AND L. EYRING, *J. Phys. Chem.* **72,** 4415 (1968).
5. H. INABA, A. NAVROTSKY, AND L. EYRING, *J. Solid State Chem.* **37,** 67 (1981).
6. H. INABA AND K. NAITO, *J. Solid State Chem.*, **50,** 100 (1983).
7. K. H. LAU, D. L. FOX, S. H. LIN, AND L. EYRING, *High Temp. Sci.* **8,** 129 (1976).
8. I. K. NAIK AND T. Y. TIEN, *J. Phys. Chem. Solids* **39,** 311 (1978).
9. J. M. HONIG, *J. Chem. Educ.* **43,** 76 (1966).
10. J. M. HONIG, A. A. CELLA, AND J. C. CORNWELL, *Rare Earth Res.* **2,** 555 (1964).
11. G. V. R. RAO, S. RAMDAS, P. N. MEHROTRA, AND C. N. R. RAO, *J. Solid State Chem.* **2,** 377 (1970).
12. G. V. CHANDRASHEKHAR, P. N. MEHROTRA, G. V. RAO, E. C. SUBBARAO, AND C. N. R. RAO, *Trans. Farad. Soc.* **63,** 1295 (1967).
13. A. LOWE, K. H. LAU, AND L. EYRING, *J. Solid State Chem.* **15,** 9 (1975).
14. A. T. LOWE AND L. EYRING, *J. Solid State Chem.* **14,** 383 (1975).
15. D. R. KNITTEL, S. P. PACK, S. H. LIN, AND L. EYRING, *J. Phys. Chem.* **67,** 134 (1977).
16. H. INABA, S. P. PACK, S. H. LIN, AND L. EYRING, *J. Solid State Chem.* **33,** 295 (1980).
17. T. SUGIHARA, S. H. LIN, AND L. EYRING, *J. Solid State Chem.* **40,** 226 (1981).
18. P. A. FAETH AND A. F. CLIFFORD, *J. Phys. Chem.* **67,** 1453 (1963).
19. M. S. JENKINS, R. P. TURCOTEE, AND L. EYRING, *in* "The Chemistry of Extended Defects in Nonmetallic Solids" (L. Eyring and M. O'Keeffe, Eds.), p. 36, North-Holland, Amsterdam, 1970.
20. H. L. TULLER AND A. S. NOWICK, *J. Phys. Chem. Solids* **38,** 859 (1977).
21. J. A. ENDERBY, *Trans. Farad. Soc.* **51,** 835 (1955).
22. S. H. LIN, M. B. LANGLEY, R. H. LANGLEY, AND L. EYRING, to be published.